Wall treatments and wall functions

A wall treatment is the set of near-wall modelling assumptions for each turbulence model. Three types of wall treatment are provided in FLUENT, although all three might not always be available, depending on the turbulence model:

• The high-y+ wall treatment implies the wall function type approach in which it is assumed that the near-wall cell lies within the logarithmic region of the boundary layer.

• The low-y+ wall treatment is suitable only for low Reynolds number turbulence models in which it is assumed that the viscous sub-layer is properly resolved.

• The all-y+ wall treatment is a hybrid treatment that attempts to emulate the high- wall treatment for coarse meshes and the low-y+ wall treatment for fine meshes. It is also formulated with the desirable characteristic of producing reasonable answers for meshes of intermediate resolution (that is, when the wall-cell centroid falls within the buffer region of the boundary layer).

The wall functions are a set of semi empirical functions used to satisfy the physics of the flow in the near wall region. Turbulence is affected in many ways by the presence of the wall through the non slip condition that must be satisfied at the wall. Four areas in the near wall region are defined, the laminar sub-layer, the blending region, the log law region and the outer region. Each region has a different effect on turbulence and a particular care must be taken to the y+ position of the first cell in the boundary layer. A different set of equations will be used depending on the size of this cell but however this one must not be comprised between y+=5 and y+=30 because no turbulent model is available in this area. Instead of not resolving the entire boundary layer for a y+ comprised in the viscous sub-layer and buffer layer, wall functions are used to bridge the viscosity-affected region between the wall and the fully-turbulent region.

Standard wall function

Standard wall functions give reasonable accuracy for a majority of high-Reynolds-number, wall-bounded flows but reach their limitation when the flow condition differ to much from the ideal conditions used to define the functions. The cases in which this limits might be reached are:

- Pervasive low-Reynolds-number or near-wall effects (e.g., flow through a small gap or highly viscous, low-velocity fluid flow)
- Massive transpiration through the wall (blowing/suction)
- Severe pressure gradients leading to boundary layer separations
- Strong body forces (e.g., flow near rotating disks, buoyancy-driven flows)
- High three-dimensionality in the near-wall region (e.g., Ekman spiral flow, strongly skewed 3D boundary layers)

The standard wall functions are made of the momentum equation which leads to the law of the wall for the temperature and depends on the y*.

$$T^* \equiv \frac{(T_w - T_P)\,\rho c_p C_\mu^{1/4} k_P^{1/2}}{\dot{q}} = \begin{cases} \mathrm{Pr}\, y^* + \frac{1}{2}\rho \mathrm{Pr} \frac{C_\mu^{1/4} k_P^{1/2}}{\dot{q}} U_P^2 & (y^* < y_T^*) \\ \mathrm{Pr}_t \left[\frac{1}{\kappa}\ln(E y^*) + P\right] + & \\ \frac{1}{2}\rho \frac{C_\mu^{1/4} k_P^{1/2}}{\dot{q}} \left\{\mathrm{Pr}_t U_P^2 + (\mathrm{Pr} - \mathrm{Pr}_t) U_c^2\right\} & (y^* > y_T^*) \end{cases}$$

Y*<Yt*: linear law for the thermal conduction sublayer where conduction is important.

Y*>Yt*: logarithmic law for the turbulent region where effects of turbulence dominate conduction.

The pressure P is computed from the formula given by Jayatilleke and the Yt* is computed as the Y* reach the linear law and the logarithmic law intersect. Depending on the Y* value at the near-wall cell, either the linear or the logarithmic profile is applied to compute the wall temperature Tw or heat flux q.

A model for flows in which chemical reactions occur is available and is known as the species transport equation but is not investigated in this report.

The turbulence model is the k-ε model where the k equation is computed over the all domain including the adjacent wall region with a boundary condition defined as follow:

$$\frac{\partial k}{\partial n} = 0$$

Where n is the local coordinate normal to the wall.

The production term is defined as follow:

$$G_k \approx \tau_w \frac{\partial U}{\partial y} = \tau_w \frac{\tau_w}{\kappa \rho C_\mu^{1/4} k_P^{1/2} y_P}$$

and ϵ is computed from

$$\epsilon_P = \frac{C_\mu^{3/4} k_P^{3/2}}{\kappa y_P}$$

Non-Equilibrium wall functions

When the near-wall flows are subjected to severe pressure gradients, and when the flows are in strong non-equilibrium, which means that the turbulence production term and the dissipation term are not equals, the results given by the standard functions are not satisfactory enough and the Non-Equilibrium wall function allows for better calculations. The equations used are:

- Launder and Spalding's log-law for mean velocity is sensitized to pressure-gradient effects.

$$\frac{\tilde{U} C_\mu^{1/4} k^{1/2}}{\tau_w/\rho} = \frac{1}{\kappa} \ln\left(E \frac{\rho C_\mu^{1/4} k^{1/2} y}{\mu}\right)$$

- The two-layer-based concept (Wall adjacent neighbouring cells consisting in a viscous sub-layer and a fully turbulent layer) is adopted to compute the budget of turbulence kinetic energy ($\overline{G_k}$, $\overline{\epsilon}$) in the wall-neighboring cells.

$$\tau_t = \begin{cases} 0, & y < y_v \\ \tau_w, & y > y_v \end{cases} \quad k = \begin{cases} \left(\frac{y}{y_v}\right)^2 k_P, & y < y_v \\ k_P, & y > y_v \end{cases} \quad \epsilon = \begin{cases} \frac{2\nu k}{y^2}, & y < y_v \\ \frac{k^{3/2}}{C_\ell y}, & y > y_v \end{cases}$$

Then using this profiles it is possible to calculate the production and dissipation terms of k with the following equations.

$$\overline{G_k} \equiv \frac{1}{y_n} \int_0^{y_n} \tau_t \frac{\partial U}{\partial y} dy = \frac{1}{\kappa y_n} \frac{\tau_w^2}{\rho C_\mu^{1/4} k_P^{1/2}} \ln\left(\frac{y_n}{y_v}\right)$$

and

$$\overline{\epsilon} \equiv \frac{1}{y_n} \int_0^{y_n} \epsilon \, dy = \frac{1}{y_n} \left[\frac{2\nu}{y_v} + \frac{k_P^{1/2}}{C_\ell} \ln\left(\frac{y_n}{y_v}\right)\right] k_P$$

The ability of the Non-Equilibrium function account for the effect of pressure gradients and departure from non equilibrium make this model more accurate and more robust for complex flows such as separated flows, reattached flows or impinging flows.

Enhanced wall functions

The enhanced function in FLUENT are used to achieve near wall modelling approach having the accuracy of the standard two layer approach for fine meshes and at the same time not degrading the results for the wall function meshes. In order to do so the enhanced wall functions are combined with the two layer model.

The two layer model is defined as a near wall model which resolves the entire boundary layer until the viscous sub-layer. The all domain is devised in two regions, a viscosity-affected region and a fully-turbulent region and the separation is determined by a wall distance defined from a Reynolds number based on y.

$$\mathrm{Re}_y \equiv \frac{\rho y \sqrt{k}}{\mu}$$

In the fully turbulent region the k- ϵ model is used whereas in the viscosity-affected near-wall region the one-equation model of Wolfstein is employed. This one equation model uses the same formulation for k and the momentum equation but the turbulent viscosity is computed, depending on the region in which the calculation is performed, from:

$$\mu_{t,\mathrm{2layer}} = \rho\, C_\mu \ell_\mu \sqrt{k}$$

$$\mu_{t,\mathrm{enh}} = \lambda_\epsilon \mu_t + (1-\lambda_\epsilon)\mu_{t,\mathrm{2layer}}$$

Kader function is used to be able to build a model which still valid throughout the near wall region, this formulation blends together the laminar and log law formulation in order to do so.

$$u^+ = e^{\Gamma} u^+_{\mathrm{lam}} + e^{\frac{1}{\Gamma}} u^+_{\mathrm{turb}}$$

Hence the law of the wall for the fully turbulent region is derived in the form:

$$\frac{du^+_{\mathrm{turb}}}{dy^+} = \frac{1}{\kappa y^+}\left[S'(1-\beta u^+ - \gamma (u^+)^2)\right]^{1/2}$$

where

$$S' = \begin{cases} 1+\alpha y^+ & \text{for } y^+ < y^+_s \\ 1+\alpha y^+_s & \text{for } y^+ \geq y^+_s \end{cases}$$

And the law of the wall for the laminar region is:

$$\frac{du_{\text{lam}}^{+}}{dy^{+}} = 1 + \alpha y^{+}$$

In the same way the thermal wall function are derived by blending together the laminar and logarithmic profiles.

Pressure distribution over the ONERA M6 wing

In order to investigate the effects of wall treatments, the pressure coefficient has been calculated with FLUENT over the ONERA M6 wing. These results have been compared with experimental data in the above plots for a set of seven sections. The three wall treatments which have been investigated are the standard wall functions, the non equilibrium wall functions and the enhanced wall functions. The sections are taken on the wing along the span wise direction, the values of Z at which the data are compared are shown below.

Section N°	Z/b in %	Z in m
1	0,2	0,23926
2	0,44	0,526372
3	0,65	0,777595
4	0,8	0,95704
5	0,9	1,07667
6	0,95	1,136485
7	0,99	1,184337

To understand the flow patterns over the wing a plane offset has been created at a short distance from the wall (0.0005m) since no velocity can be capture at the wall due to the no-slip condition. This transformed plane enables to visualize the velocities near the wall and so to capture the shock position and pattern. The stream lines have also been plotted to give an idea of the flow migration.

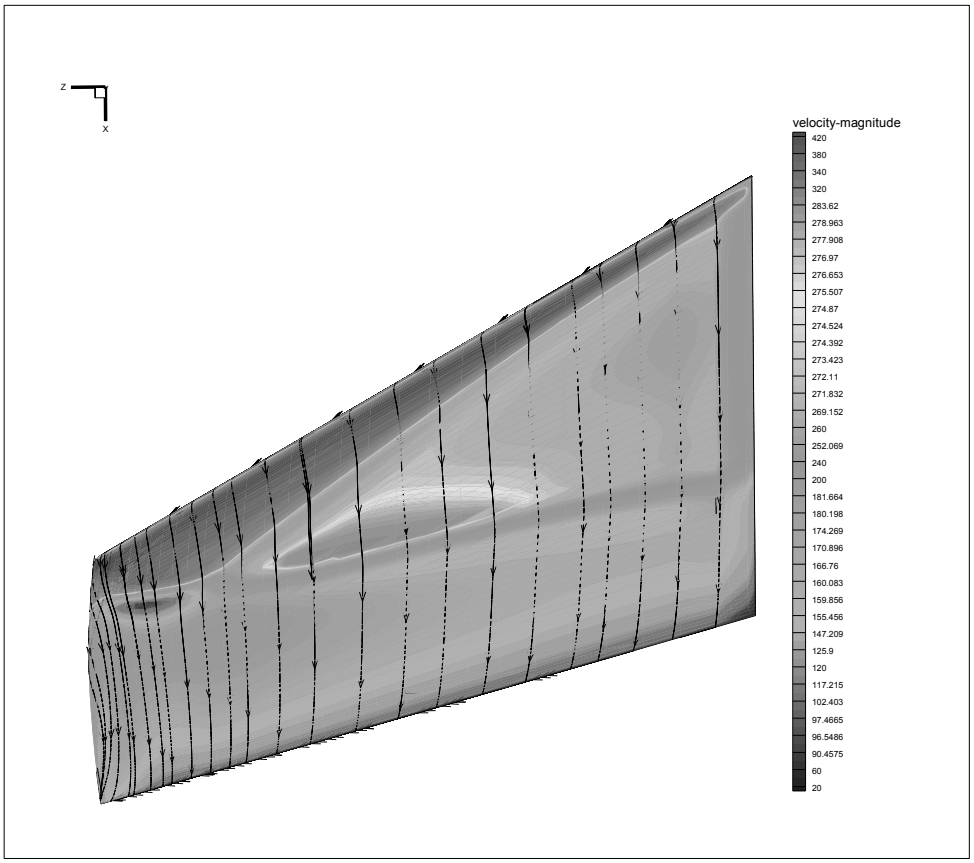

Figure 1: Velocities on the transformed plane over the ONERA M6 wing

From this plot it is possible to see that a lambda shock forms on the upper surface and coalesces into a normal shock at about 80% of the span close to the tip. This is reflected in the Cp plots in which we can clearly see the two shocks for section 1, 2, 3 and 4 (Figure 1, Figure 3, Figure 4, Figure 5). For these sections, the flow is accelerated at the leading edge until they encounter the first swept shock which reduces the flow velocity. The flow then again accelerates because of the airfoil curvature and is decelerated by the second shock. For section 5, 6 and 7 (Figure 6, Figure 7 and Figure 8) the flow is accelerated around the leading edge and encounters a normal shock which is much stronger that the swept shock and strongly reduces the velocity. It is very likely that this shock generates separation of the flow but this is not seen in the results. The other data present on this figure are the stream traces and it is possible to see that in the root region the stream traces follow the x axis direction whereas when moving toward the tip the traces are distorted and form an S shape due to flow migration span wise. Toward the tip the flow migration from the lower surface to the upper surface induced by the difference in pressure lead to high 3D effect in the boundary layer at the tip and might lead to difficulties for resolving the boundary layer.

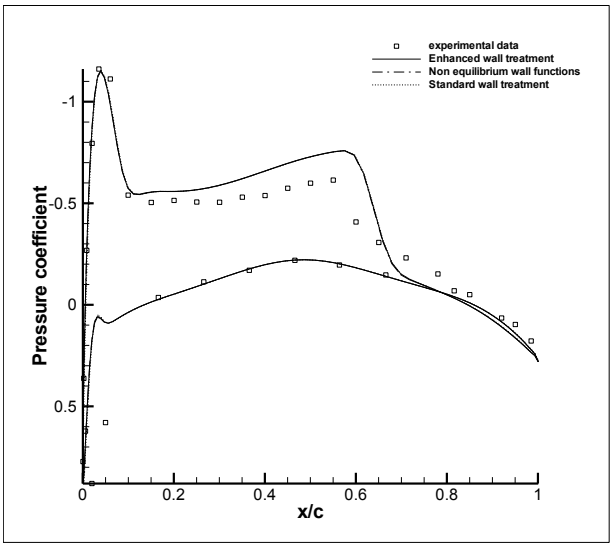

Figure 2: Pressure coefficient comparison for section 1

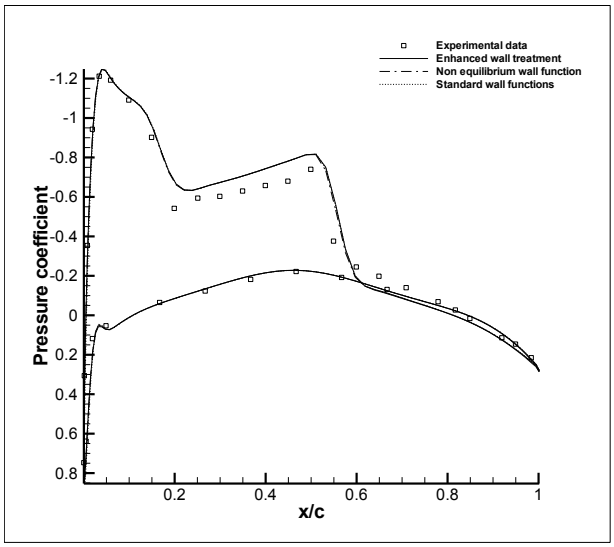

Figure 3: Pressure coefficient comparison for section 2

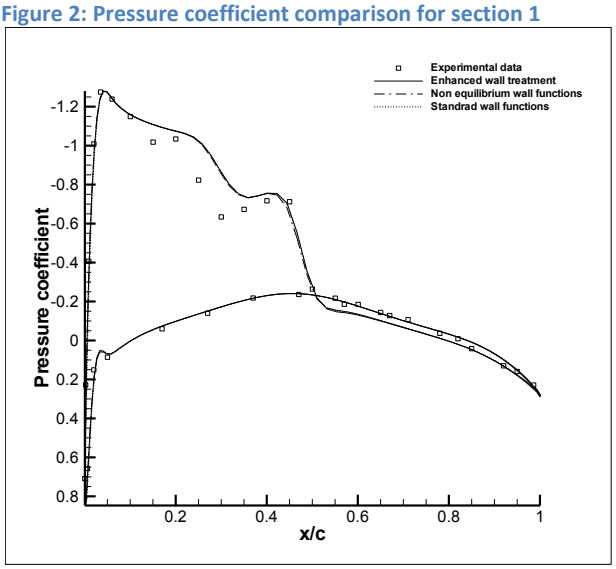

Figure 4: Pressure coefficient comparison for section 3

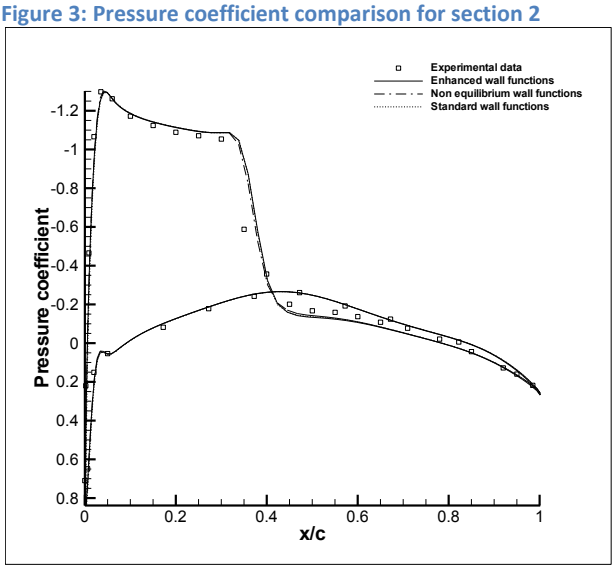

Figure 5: Pressure coefficient comparison for section 4

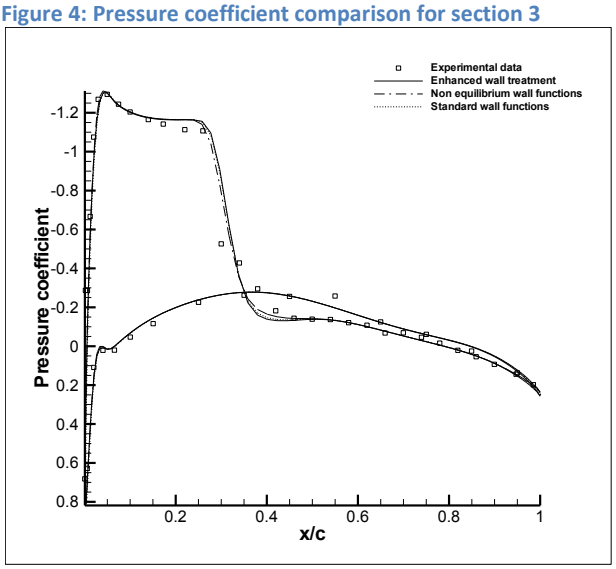

Figure 6: Pressure coefficient comparison for section 5

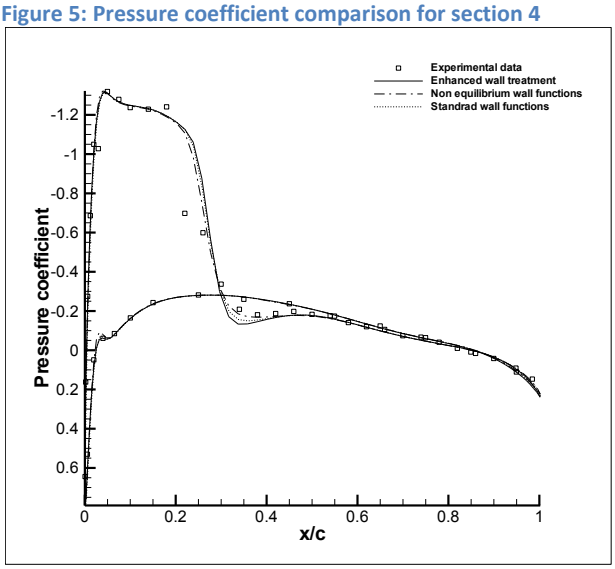

Figure 7: Pressure coefficient comparison for section 6

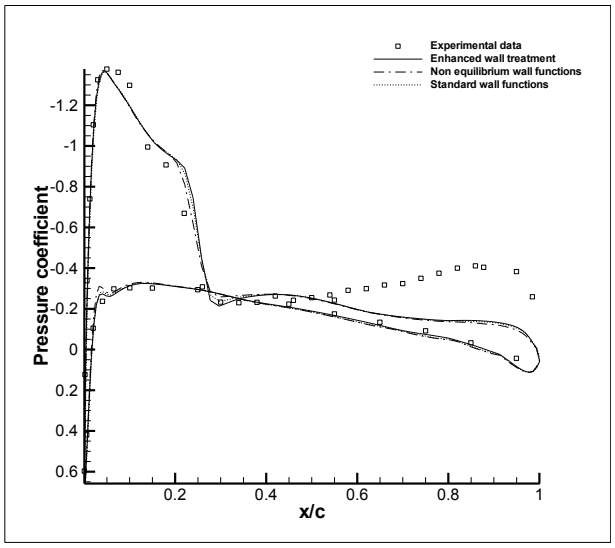

Figure 8: Pressure coefficient comparison for section 7

The calculation done with the three different wall treatment yields to very similar result in pressure coefficient and no conclusion can be drawn from this analysis. Although the results are in accordance with the experiment it is possible to see that for section 3 the FLUENT calculation does not capture clearly the two pattern shock, the solution is quite diffusive. For section 1, 2 and 3 the region in-between the shocks is no really well predicted. The Cp in this region is slightly higher than the experimental data which means that more suction is generated than in reality.

A mean of explaining this observation is to say that the wall functions are active in the viscous regions hence the boundary layer. Those functions will have an effect on the prediction of the velocity profile within the boundary layer and so will affect the displacement thickness and the viscous shears. Differences in the displacement thickness for each wall treatment are less important than the differences in shear stress and that is why no difference can be seen between the different functions. However this difference in displacement thickness can modify the camber line of the airfoil section and so modify the Cp distribution. In this particular case it seems that the boundary layer displacement thickness is underestimated and so the camber of the airfoil is not reduced as it is in reality resulting in a higher suction region. This explanation would explain in the same way the difference in recovery pressure at the trailing edge which is higher than in the experimental data. Indeed if the velocity profile is mist calculated the wake will differ and in this case will be thinner allowing for a better recovery in pressure.

The velocity profile mist calculation can be explained by the poor grid resolution close to the wall which doesn't match the requirements for wall treatments. This can be seen in the Y+ plot for each section of the wing and it is clearly remarkable that the wall unit for a majority of the chord is comprised between Y+=5 and Y+=30 (Figure 9) which is the blending region. The FLUENT user's guide advice to make sure that wall units are over 30 or under 5 for a good resolution of the boundary layer because no model is available for the blending region and so a resolution in this region will yield wrong results of the velocity profiles. As none of the Y+ is under 5 then the viscous sub layer is not resolved.

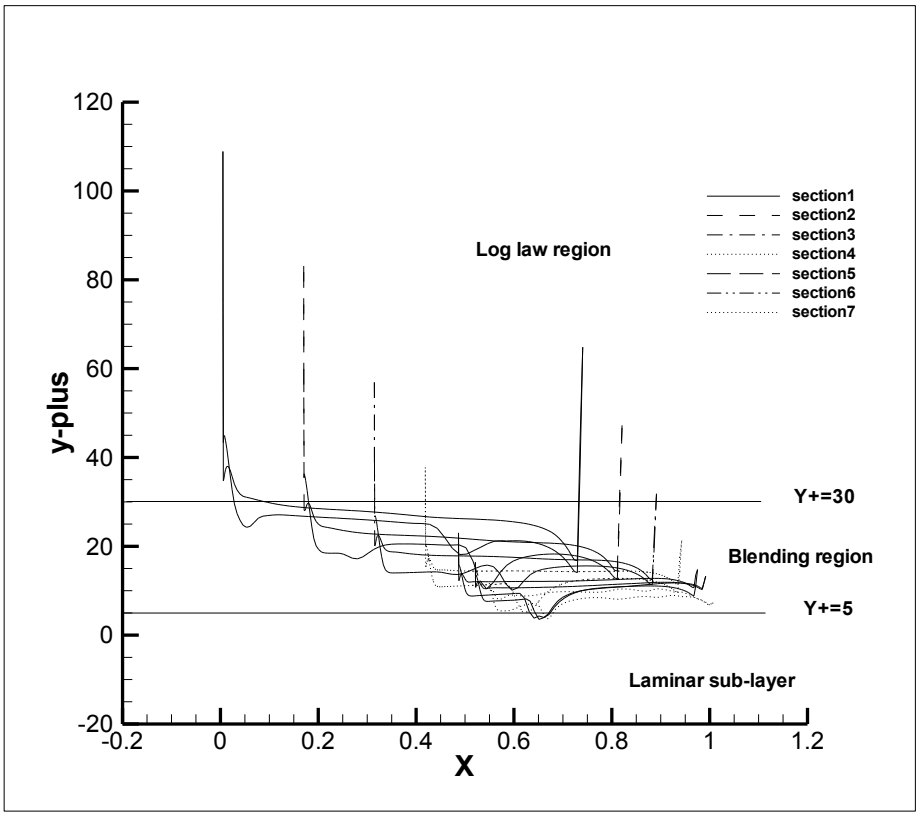

Figure 9: Y+ distribution along the chord of the airfoil

As nearly no differences can be seen between the three wall treatment the shocks positions are the same for each one of them and are summarized in the table below with the experimental data.

	Section 1		Section 2		Section 3		Section 4	Section 5	Section 6	Section 7
	forward	Haft	forward	Haft	forward	Haft				
Shock position for the FLUENT calculation (% of the section chord)	5	60	15	52	25	42	35	35	27	25
Shock position for the experimental data	5	55	10	50	20	45	32	32	27	20
Errors in %	0	5	5	2	5	-3	3	3	0	5

Skin friction coefficients

To investigate the effects of wall treatments it is interesting to look at the skin friction coefficient repartition along the sections of the wing. As it has already been said the effects of the different wall treatments are more accentuated for this coefficient than for the Cp distribution because it is directly dependant on the velocity profile.

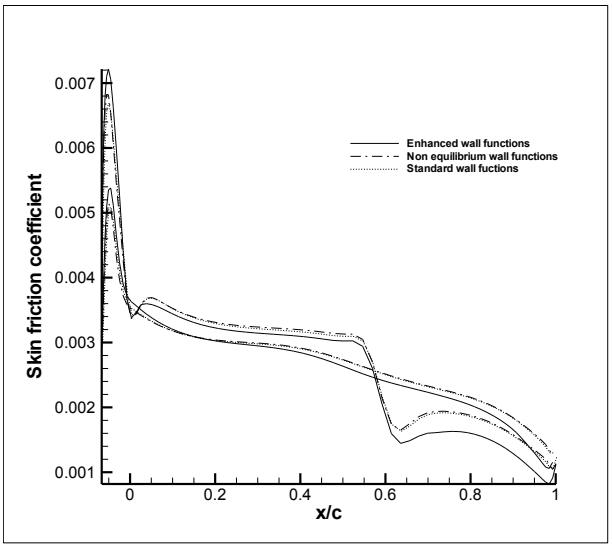

Figure 10: Skin friction coefficient for section 1

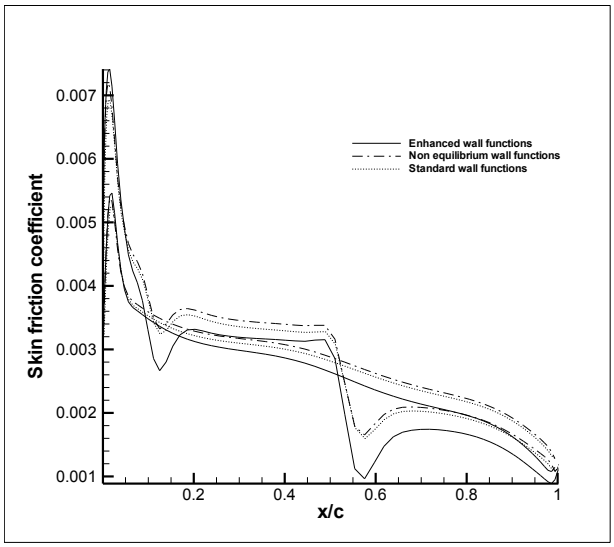

Figure 11: Skin friction coefficient for section 2

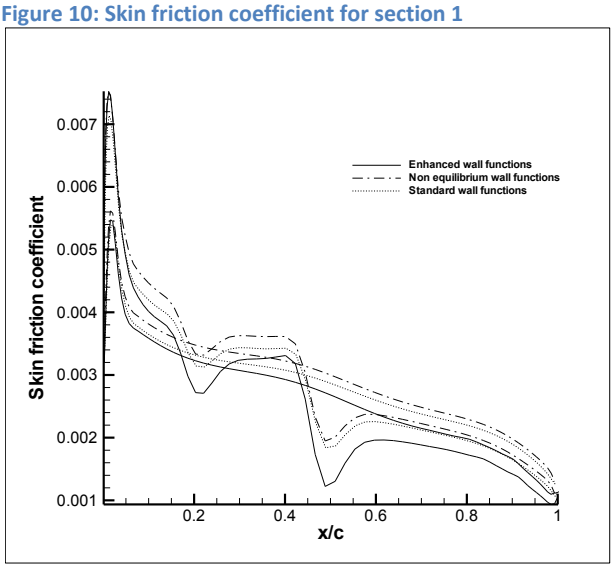

Figure 12: Skin friction coefficient for section 3

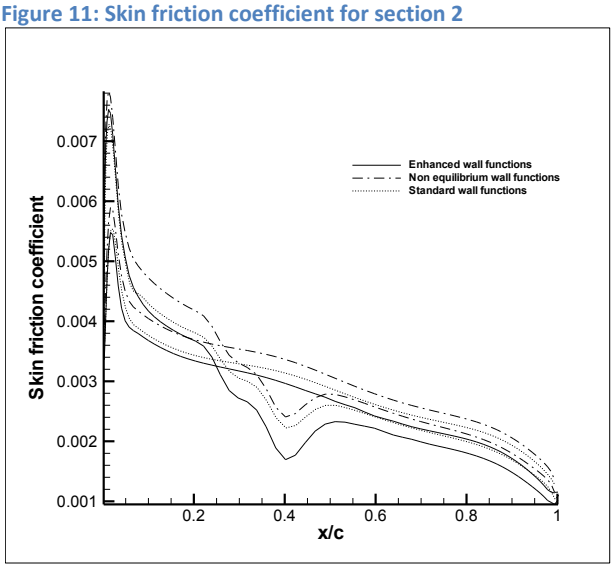

Figure 13: Skin friction coefficient for section 4

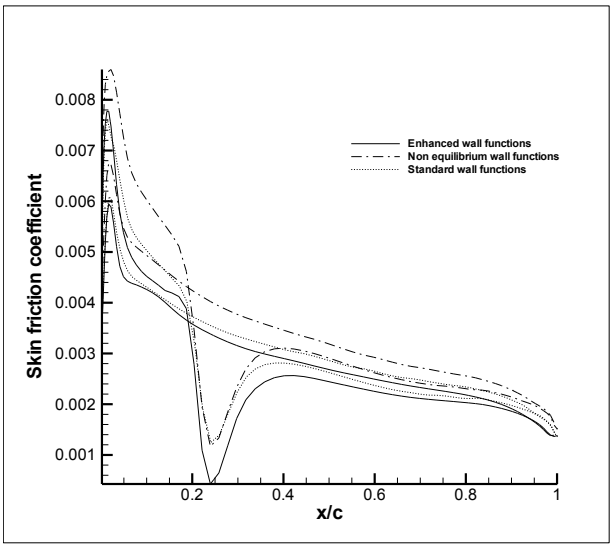

Figure 14: Skin friction coefficient for section 5

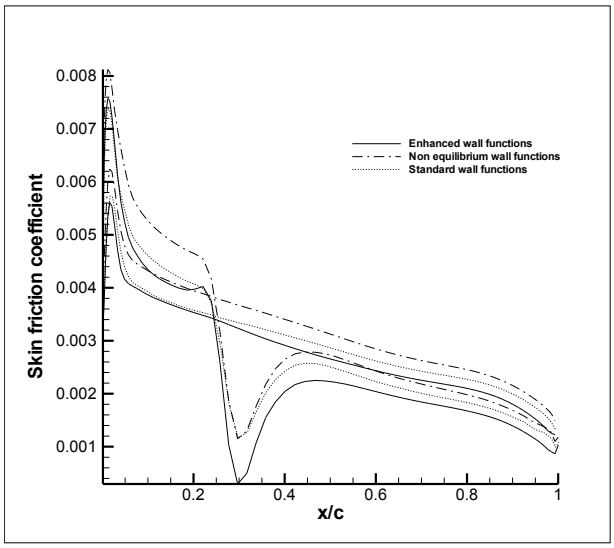

Figure 15: Skin friction coefficient for section 6

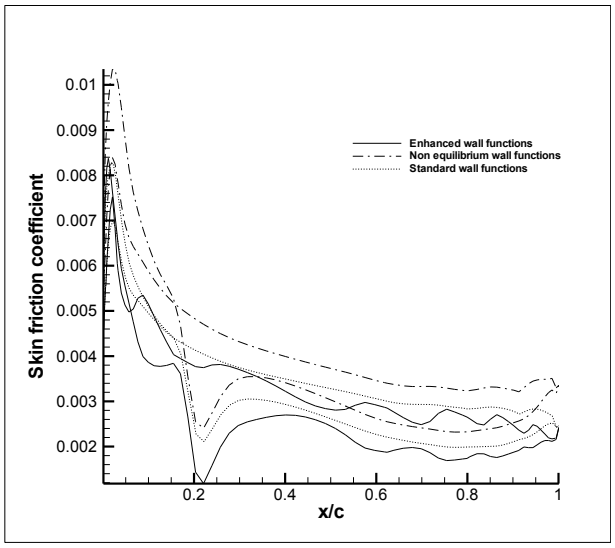

Figure 16: Skin friction coefficient for section 7

The skin friction coefficient is a good indicator to observe the shock and boundary layer interaction. As separation occurs the velocity goes to zero and so does the skin friction coefficient, however in this case no separation occurs. For section 5, 6 and 7 closer to the tip it is possible to see that the skin friction coefficient drops rapidly after the shock and is very close to zero, the flow is at the edge of separation. As there are no experimental data to be compared with the CFD calculations it is not easy to tell which wall treatment is the more accurate. Nevertheless it is known that after a strong normal shock the flow is likely to separate and so the model which predicts this behaviour in the better way is the enhanced wall treatment because the skin friction drops close to zero. Then the standard function and the non equilibrium functions are less accurate respectively. This result is a bit surprising because the non equilibrium treatment was expected to yield better results than the standard functions since it is made to capture with a better accuracy complex flows, however this can be due to the poor resolution of the mesh in the near wall region.

Velocity distribution

In order to investigate the shock and boundary layer interaction across the span wise direction of the wing and to compare the differences between the different wall treatments the velocity distribution has been plotted for the sections 1, 3 and 6.

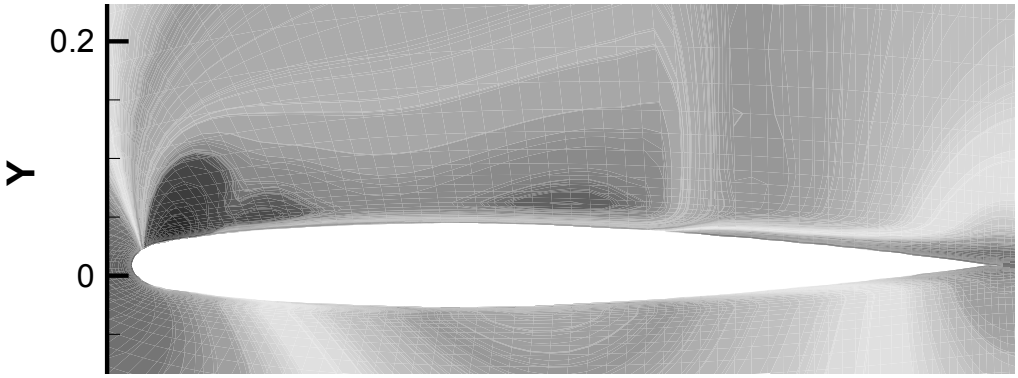

Figure 17: Velocity distribution over the airfoil for section 1 for the enhanced wall treatment

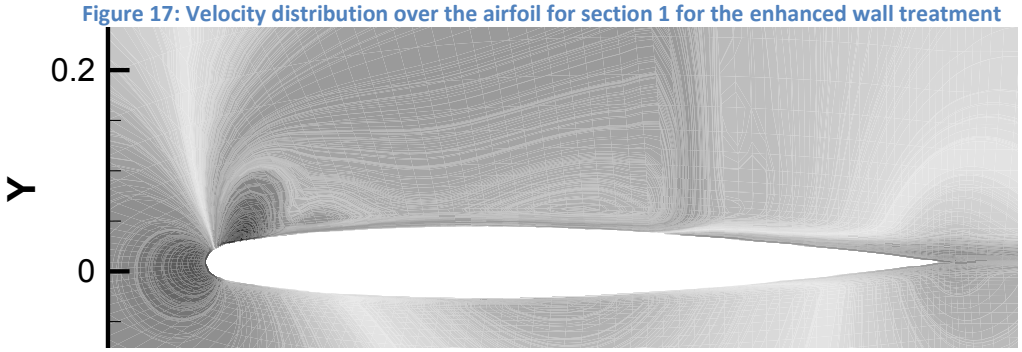

Figure 18: Velocity distribution over the airfoil for section 1 for the non equilibrium wall treatment

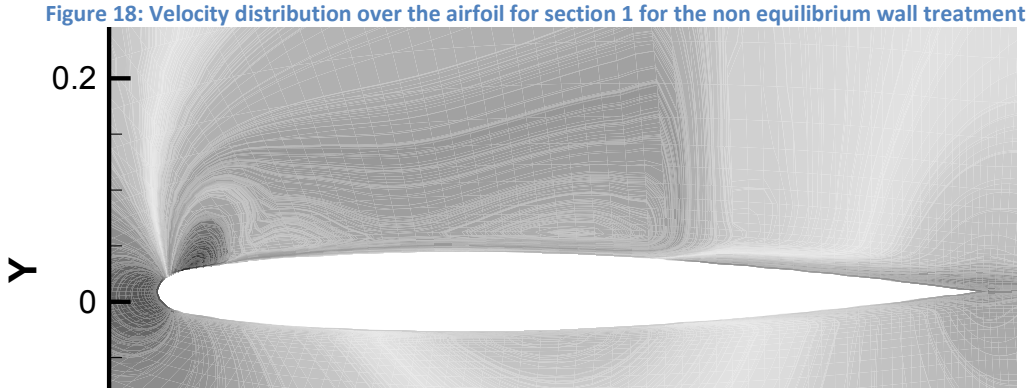

Figure 19: Velocity distribution over the airfoil for section 1 for the standard wall treatment

It is possible to see that after each shock the boundary layer thicken but none of the wall treatment predicts separation. The models predict very similar shock and boundary layer interactions with a small thickening of the boundary layer after the first shock which tend to prove that the first shock is weak. The second shock generates a greater thickening which means that the shock is stronger.

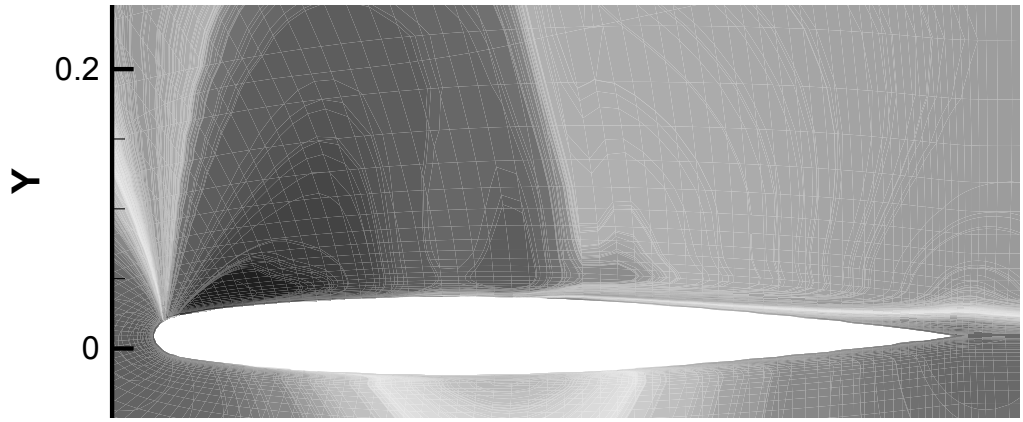

Figure 20: Velocity distribution over the airfoil for section 3 for the enhanced wall treatment

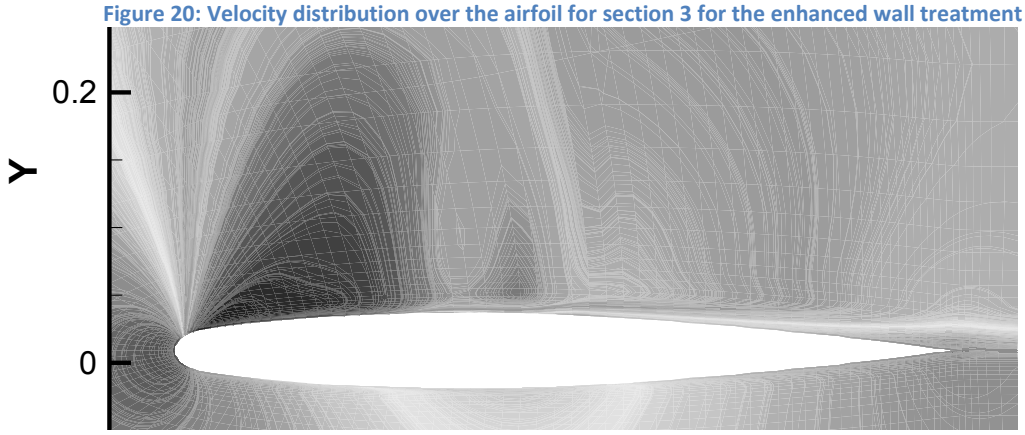

Figure 21: Velocity distribution over the airfoil for section 3 for the non equilibrium wall treatment

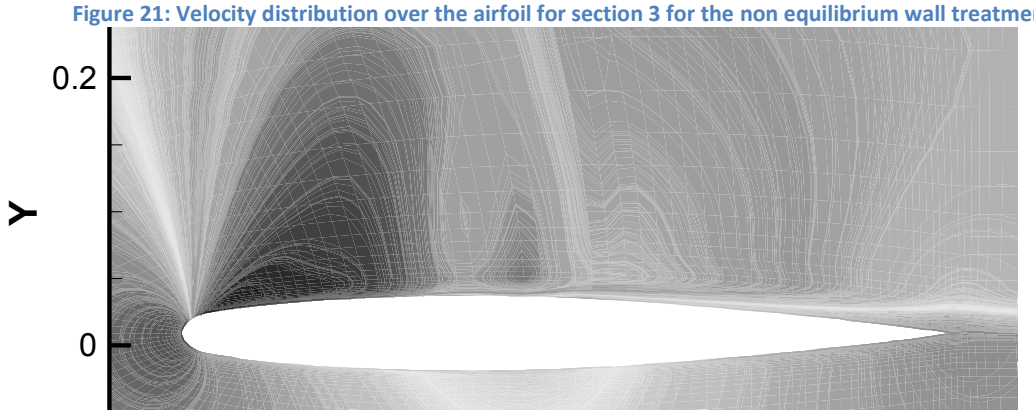

Figure 22: Velocity distribution over the airfoil for section 3 for the standard wall treatment

For section 3 which is situated at 65% of the span there are still two shocks but they are much closer and interaction is more important. Now the first shock is stronger than for section 1 and the thickening of the boundary layer is greater. In between the two shocks the favourable pressure gradient reduces the thickness of the boundary layer which increases rapidly just after the second shock. In this section no separation is observable and the three models predict the same pattern of shock and boundary layer interaction.

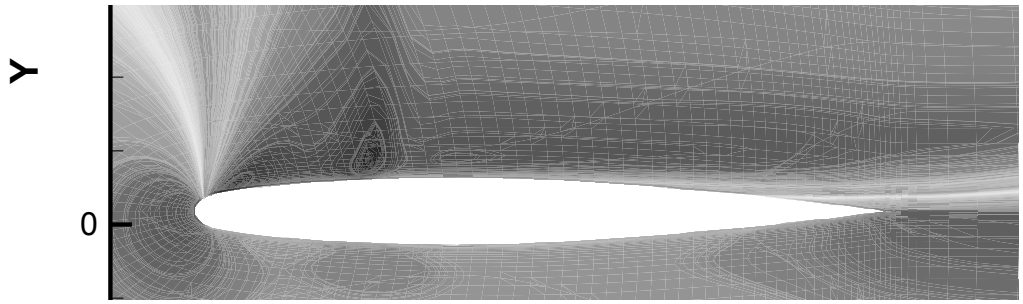

Figure 23: Velocity distribution over the airfoil for section 6 for the enhanced wall treatment

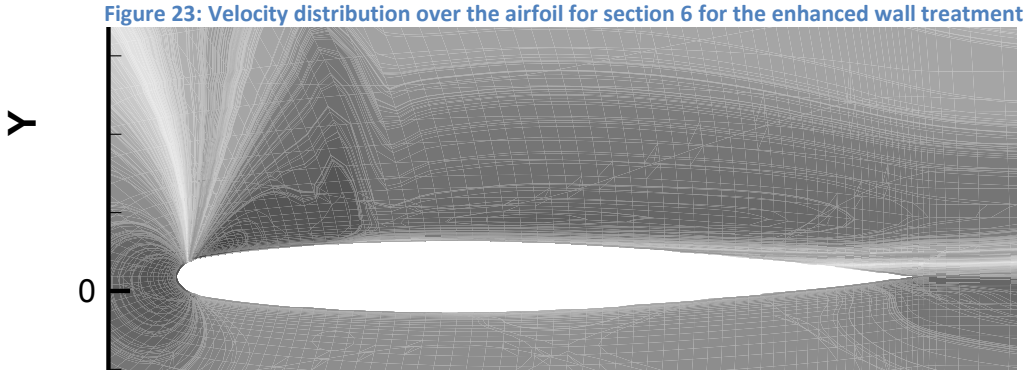

Figure 24: Velocity distribution over the airfoil for section 6 for the non equilibrium wall treatment

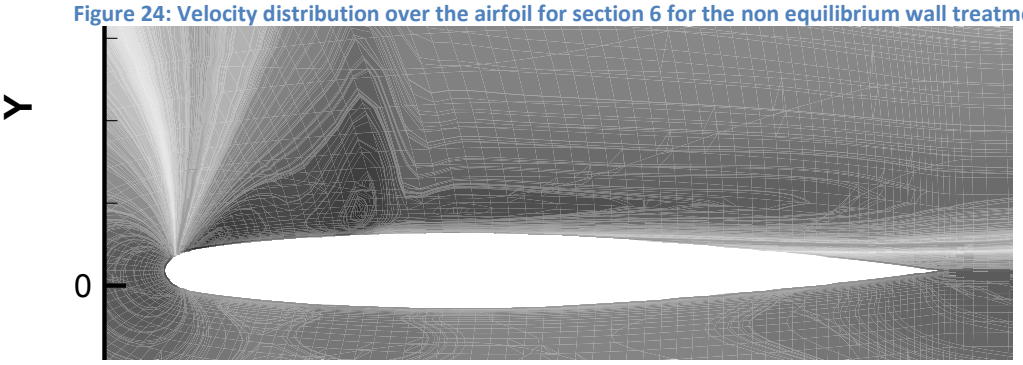

Figure 25: Velocity distribution over the airfoil for section 6 for the standard wall treatment

For section 6 only one shock remains, this shock is a strong normal shock situated at the 25% of the chord. It generates a high thickening of the boundary layer which spread toward the trailing edge; it is possible to see that the boundary layer is at the edge of separation but does not actually separates. The three treatments yield the same results and no significant differences can be noticed.

Conclusion

This study has enable to investigate the pressure distribution of an ONERA M6 wing at a Mach number of 0.83 for an angle of attack of 4° and compare it to experimental data. This study has also focused on the shock position and shock boundary layer interaction highlighting a lambda shock pattern with no induced separation. Three wall treatments have been used in order to define the best model for this particular problem and the main difference has been observed in the skin friction coefficient.

The CFD results have yield results in accordance with theory, however the grid resolution in the near wall region is not really optimised because it is situated in the $5<y+<30$ region in which the models are not very accurate. For this case the model which gives the best results is the enhanced wall treatment.